Materials Science-Poland, 40(1), 2022, pp. 196-205
http://www.materialsscience.pwr.wroc.pl/
DOI: 10.2478/msp-2022-0020

Study of synthesis parameters on the physical properties and morphology of smart PNIPAAm hydrogels

Luíza Braga Ferreira dos Santos, Francielly Moura de Souza Soares, Emília Santos Monteiro, Maria Elisa Rodrigues Coimbra, Carlos Nelson Elias*

Biomaterials Laboratory: Department of Materials Science, Military Institute of Engineering, Rio de Janeiro, Brazil

Bone loss is common in human old age and new materials that promote bone regeneration are an active line of research. In the present work, seven smart hydrogels based on PNIPAAm were synthesized with the prospective to be used in tissue engineering as a scaffold for bone growth. By changing the stoichiometric concentrations of the reagents and the synthesis parameters, hydrogels with different physical properties and morphology were obtained. Swelling, degradation properties, and crystallinity were analyzed. Physical properties were characterized using ^{1}H-NMR, FTIR, and TGA. The results showed that the swelling degree (degree of mass expansion) varied at room temperature from 1,400% for less rigid hydrogels to 550% for stiffer hydrogels. With heating to body temperature, swelling decreases to 300% and 200%, respectively. The samples presented three-dimensional morphology, but they acquired different structures according to the magnetic stirring during the synthesis process. The crosslink and initiator concentrations have an important effect on the polymeric structure and thermal stability of the hydrogels. The PNIPAAm synthesized using 8.9 and 15.7 mol % of MBA are the most promising compounds to be used in the future as a scaffold for biomedical applications due to their high thermal stability, satisfactory 3D surface morphology, and shrinking-swelling property.

Keywords: *Smart hydrogels, PNIPAAm, biomaterials, polymer gels, synthesis*

I. Introduction

Disease, injury, and trauma can lead to damage and degeneration of bone in the human body, which require repair, replacement, or regeneration [1]. The search for new materials to treat and/or stimulate the regression of a disease is a continuous endeavor [2]. Nowadays, the percentage of elder people is increasing, and there is a higher incidence of bone loss, leading in many cases to osteoporosis [3]. Global Burden of Disease (GBD) data have shown that approximately 1.71 billion people globally have musculoskeletal conditions, which include joints (osteoarthritis, rheumatoid arthritis, psoriatic arthritis, gout, ankylosing spondylitis), bones (osteoporosis, osteopenia, and associated fragility fractures, traumatic fractures), muscles (sarcopenia), and spine (back and neck pain) [4]. Factors that contribute to bone loss include lack of exercise, a diet low in calcium, smoking, and some medications such as corticosteroids, which are prescribed for a wide range of diseases, including asthma, arthritis, inflammatory bowel disease, and lupus.

Smart biomaterials have significantly expanded the boundaries of modern materials for medicine applications [5, 6]. Among them are the hydrogels with water-insoluble crosslinked three-dimensional polymer networks whose microstructure is similar to that of natural tissues [7, 8]. Besides tissue engineering, they can be used for other biomedical purposes, such as imaging, drug delivery, and scaffolds [9–12]. One of these smart materials is PNIPAAm, a group of thermosensitive hydrogel based on N-isopropyl acrylamide monomer. These hydrogels have a lower critical solution temperature (LCST) close to 32°C [2]. At temperatures below LCST, they are partially soluble in water; above LCST they become insoluble. This reversible behavior (the collapse of the swollen polymer matrix when the temperature exceeds LCST in an aqueous solution) and a critical temperature close to that of the human body becomes these materials in-

* E-mail: francielly.metalurgia@gmail.com

© 2022. This is an open access article distributed under the Creative Commons Attribution-NonCommercial-NoDerivatives 4.0 License. (http://creativecommons.org/licenses/by-nc-nd/4.0/)

teresting for medical applications [13]. PNIPAAm exhibits advantageous properties such as biocompatibility and nontoxicity. Moreover, it is possible to obtain PNIPAAm with different characteristics by varying preparation conditions such as the monomer concentration, the synthesis procedure, the type of reticulate agent, and/or the initiator [2, 13].

The purpose of this work was to investigate the influence of several synthesis parameters on the properties of PNIPAAm. The compounds were synthesized under different conditions. The PNIPAAm composition, morphology, crystalline structure, and thermal properties were analyzed by the Nuclear Magnetic Resonance Spectroscopy (NMR), Fourier Transform Infrared spectroscopy (FTIR), Energy Dispersive Spectroscopy (EDS), Thermogravimetric Analysis (TGA), X-Ray Diffractometry (XRD), and Scanning Electron Microscope (SEM). Seven hydrogel scaffold groups were synthesized with different properties that show good potential to be used as a scaffold for biomedical applications in the future. There are no studies in the literature that analyze the influence of some synthesis parameters, such as crosslink agent concentration plus initiator concentration on the PNIPAAm hydrogel properties and evaluate the synthesis process when it is used for magnetic stirring or repose during the polymerizing reaction.

II. Materials and Methods

II.1. Synthesis of PNIPAAm

In the present work, three parameters were changed in the synthesis of PNIPAAm: the crosslinker agent, initiator concentrations, and magnetic agitation.

The monomer used was N-isopropylacrylamide (NIPAM), supplied by Sigma-Aldrich. The crosslinker was N-N'-methylen(bis)acrylamide (MBA), supplied by Sigma-Aldrich and the initiators were ammonium persulphate (APS) (Gold FM), and sodium metabisulphite (NMB) (Farmos).

The PNIPAAm synthesis was performed in an aqueous solution under a nitrogen atmosphere as prescribed by Queiroz [14]. NIPAM and MBA were weighed, diluted in approximately 5 mL of deionized water, and placed in a 50 mL glass balloon. The balloon was closed and placed in a nitrogen atmosphere for 5 min. The initiators APS and NMB were weighed and diluted in approximately 5 mL of deionized water. This solution was added to the glass balloon. The reaction was placed in water at 50°C. Seven hydrogel groups were prepared with the concentration shown in Table 1. The H1.A, H2.A, and H3A hydrogel groups were prepared with magnetic stirring during the polymerization reaction. The H1.0, H2.0, H3.0, and H4.0 hydrogel groups stayed in repose, without magnetic stirring, during the polymerization reaction. Table 1 shows that the concentrations of H1.0, H2.0, and H3.0 groups are the same as the H1.A, H2.A, and H3.A groups, and the difference among them was the synthesis process. The gelation started 30 s and 1 min after the introduction of the last reagent, varying according to the crosslinking ratio, being that it was inversely proportional to crosslink concentration. During this process, the solution changed from transparent to milky and viscous. After gelation, the samples stayed at room temperature for 24 h to complete the reaction. After that time, the samples were washed three times with approximately 15 mL of deionized water in a centrifuge at 3,500 rpm to eliminate any residues, and then they were placed in an oven at 60^{o}C to remove residual water. The reagent concentrations in mmol and mol % are shown in Table 1.

II.2. Swelling ratio (Q)

The swelling ratio, also called the mass expansion ratio, is used to relate the mass of the water-swollen hydrogel (M_{ge}) to the mass of the dry hydrogel (M_g) [15]. It is given by the following equation 1 [16, 17]:

$$Q = [(M_{ge} - M_g)/M_g] \times 100\% \qquad (1)$$

Approximately 250 mg of each dry sample were placed in a 50 ml beaker, which was filled with Phosphate Buffered Saline (PBS) solution to 30 mL to let the gels expand at room temperature (25°C) and 37°C. After the time of 1, 5, 10, 15, 20, 30,

Table 1. Hydrogel groups, reagents concentration, and synthesis process

Groups	NIPAM (mmol)	MBA (mmol)	APS (mmol)	NMB (mmol)	Mol %	Magnetic stirring
H1.A*	2.21	0.135	0.078	0.097	87.7×5.4×3.1×3.8	Yes
H2.A*	2.26	0.239	0.074	0.101	84.5×8.9×2.8×3.8	Yes
H3.A*	2.22	0.446	0.059	0.076	79.3×15.9×2.1×2.7	Yes
H1.0	2.21	0.132	0.076	0.097	87.8×5.2×3.2×3.8	No
H2.0	2.22	0.235	0.075	0.102	84.4×8.9×2.8×3.9	No
H3.0	2.23	0.443	0.057	0.074	79.5×15.8×2.3×2.6	No
H4.0	2.22	0.443	0.076	0.075	78.9×15.7×2.8×2.6	No

*The letter A means that the sample was synthesized utilizing magnetic stirring in the process.

40, 50, 60, 80, 100, 120 min, the samples were removed from the beaker, dried with filter paper to remove the surface water, and weighed. To determine the dry mass, M_g, the samples were put in an oven at 60°C for 24 h before weighing. This experiment was carried out in triplicate.

II.3. Nuclear Magnetic Resonance Spectroscopy (NMR)

Physical properties were characterized using ^{1}H-NMR spectroscopy to determine the number of hydrogen atoms in the sample molecules. The ^{1}H spectra were recorded in a Varian VNMRS spectrometer operating at a frequency of 500 MHz. The measurements were performed after the samples had been immersed for 25 min in deuterated water (D_2O) solvent, with a hydrogel/solvent ratio of 1:4 w/w. The temperature was about 30°C, and the spectra were collected on a preset mode to suppress the D_2O peak. The chemical dislocations (δ) were expressed as parts per million (ppm).

II.4. Fourier Transform Infrared spectroscopy (FTIR)

FTIR spectra were performed in a Varian 660 IR spectrometer in the 400–4,000 cm^{-1} range using specular reflection [18]. The spectra were collected at room temperature with a nominal resolution of 4.00 cm^{-1} and 32 scans, using the attenuated total reflectance (ATR) accessory. Approximately 3 mg of dry hydrogel powder was used in this analysis.

II.5. Energy Dispersive Spectroscopy (EDS)

Assessment of the hydrogel composition was performed by energy dispersive spectroscopy (EDS) at various magnifications and accelerating voltages at randomly selected spots, using a Bruker detector controlled by Quantax CrystAlign Software attached to an FEI Quanta FEG 250 SEM.

II.6. X-Ray Diffraction (XRD)

XRD powder diffraction patterns (XRD) were recorded in a Bruker-AXS D8 Advance diffractometer, from 5° to 60° (2θ) with a step size of 0.02 at room temperature, using a Cu Kα ($\lambda = 0.154$ Å) radiation source. Before the measurement, the samples were macerated to avoid a preferential orientation. The X'Pert Data Viewer software was used to compute the areas of the amorphous halo (A_a) and the crystalline peaks (A_c) to estimate the degree of crystallinity *(X_C)* of the hydrogels using the following equation 2, proposed by Ruland [19]:

$$X_c = (A_C/A_a + A_c) \times 100\% \qquad (2)$$

II.7. Scanning Electron Microscopy (SEM)

Before SEM measurements, the samples were immersed for 24 h in deionized water, placed in liquid nitrogen for 1 min, freeze-dried for 3 days for complete water removal, and sputter-coated by platinum to enhance conductivity. The surface morphology was studied using an FEI Quanta FEG 250 SEM.

II.8. Thermogravimetric Analysis (TGA)

TGA measurements were performed using a TA Instruments Q500 thermogravimetric analyzer. Approximately 5 mg of each sample were placed in a platinum crucible and heated at a rate of 5°C/min from 25°C to 600°C in a nitrogen atmosphere. The first derivative of the TGA curve (DTA) was computed for better visualization of the thermal behavior of the samples.

III. Results and Discussion

Macroscopically, different morphologies were observed in hydrogels synthesized with and without stirring, even though all displayed a white color, like that of the one shown in Figure 1. A film was formed in hydrogels synthesized without stirring and small agglomerates in hydrogels synthesized with stirring. This difference influenced the XRD and SEM results, but all samples exhibited the same bands in FTIR and RMN spectra, showing that all samples have the same chemical composition.



Fig. 1. Sample H1.0 after gelation

III.1. Swelling Ratio (Q)

Figure 2 shows the oscillatory shrinking-swelling property of the PNIPAAm hydrogels. The oscillation became less pronounced when the samples were heated to 37°C because of the LCST effect. The hydration/dehydration kinetics of H2.0 and H4.0 samples remained stable for 60 min and presented less variation of swelling ability than the samples H1.0 and H3.0 due to the higher concentration of MBA and APS, which increased the rigidity of the hydrogels. As the H1.0 and H1.A have lower MBA concentrations, they have higher swelling and oscillatory shrinking-swelling capacity, being the less rigid hydrogels, in order words, they have a high capacity to incorporate water inside their structures.

As crosslink reagent concentration increased, more rigid was the polymer structure, and the less was the swelling capacity. This behavior is the consequence of the number of bridges formed on the polymeric structure. On the other hand, comparing H3.0 with H4.0 groups, which differ only in the APS concentration, one notices that the H4.0 sample, which has a higher APS concentration, is more rigid, showing that the redox initiator has an important rule to facilitate crosslinking. It was observed that the magnetic stirring during the synthesis process was important to determine the hydrogels' behavior. The H1.A, H2.A, and H3.A groups showed a great oscillatory swelling capacity. The magnetic stirring could have contributed to forming polymeric chains of different sizes and crosslinking degrees.

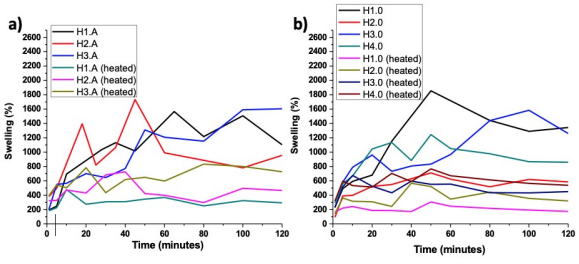


Fig. 2. Swelling ratios of the hydrogels at room temperature and 37°C in (a) stirred samples and (b) unstirred samples

III.2. Chemical Analysis

Table 2 shows the NMR analysis was performed in H1.0, H2.0, H3.0, and H4.0 unheated samples because they were the ones with the largest swelling.

The chemical shifts are similar in all four unheated hydrogel samples (Figure 3) and did not show the peaks at 5.80 and 6.27 ppm that appear in the Nipam spectrum. According to Wang et al. [21],

Table 2. NMR ^{1}H Spectra results

Groups	Chemical dislocation (ppm)	Integration ratio/number of hydrogens involved
H1.0	1.22	6.04 / 6
	1.66	1.89 / 2
	2.09	1.17 / 1
	3.98	1.00 / 1
H2.0	1.08	6.00 / 6
	1.64	2.19 / 2
	1.96	1.17 / 1
	3.83	1.16 / 1
H3.0	1.22	5.93 / 6
	1.78	1.98 / 2
	2.10	1.33 / 1
	3.97	1.00 / 1
H4.0	1.21	6.00 / 6
	1.68	2.32 / 2
	2.11	1.12 / 1
	3.98	0.85 / 1

the multiplet at about 1.2 ppm is due to a methyl group (CH_3), the multiplet at about 1.7 ppm is due to a methylene group (CH_2), the multiplet at about 2.1 ppm is associated with hydrogen close to the oxygen of an amide group, and the multiplet at about 4.0 ppm is due to one hydrogen atom close to the nitrogen of an amide group. It was previously mentioned that when a hydrated hydrogel is heated at temperatures close to the LCST, some water molecules are expelled from the polymer network to form free water (FW). The remaining water in the polymer is named confined water (CW). That is why the H4.0 sample, which has the highest crosslink concentration, exhibits the largest CW peak. The peaks labeled * in the spectra are due to rotational sidebands. The hydrogen of the amide group did not appear on spectra, probably because it was associated with interchangeable hydrogen atoms of the D_2O solvent [20, 21].

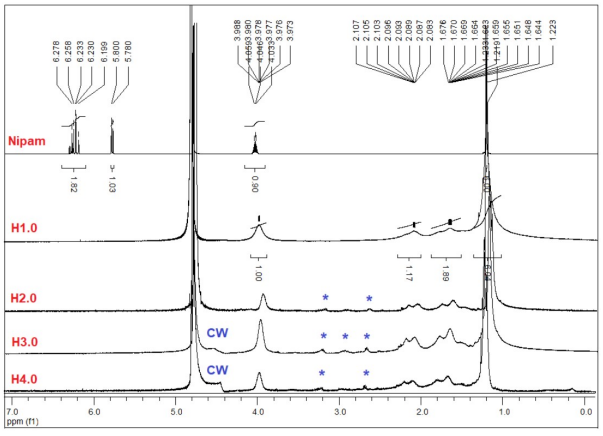


Fig. 3. ^{1}H NMR spectra of Nipam, H1.0, H2.0, H3.0, and H4.0 (500 MHz, D_2O).

Figure 4 shows the ATR-FTIR spectra of the hydrogels. All samples showed a band at 3,285 cm^{-1} associated with stretching and a band at 1,535 cm^{-1} associated with angular deformation of the N-H bond of secondary amide. The band at 3,080 cm^{-1} is attributed to the unfolding of the N–H bond. The absence of a peak between in the 1,675–1,645 cm^{-1} interval, which would be associated with the C=C bond, means there was no residual of NIPAM monomer in the hydrogels. The bands at 2,865, 2,930, and 2,974 cm^{-1} are related to C–H stretching and the one at 1,623 cm^{-1} is characteristic of the C=O stretching of carbonyl amide. Angular deformation of the C-H bond of methyl and isopropyl groups can be observed at 1,456 and 1,376 cm^{-1}, respectively.

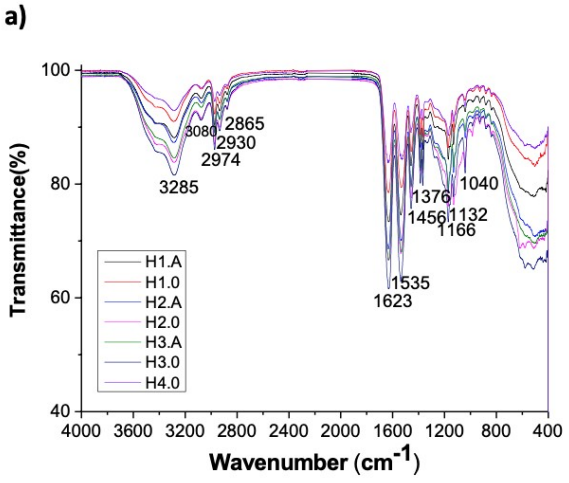
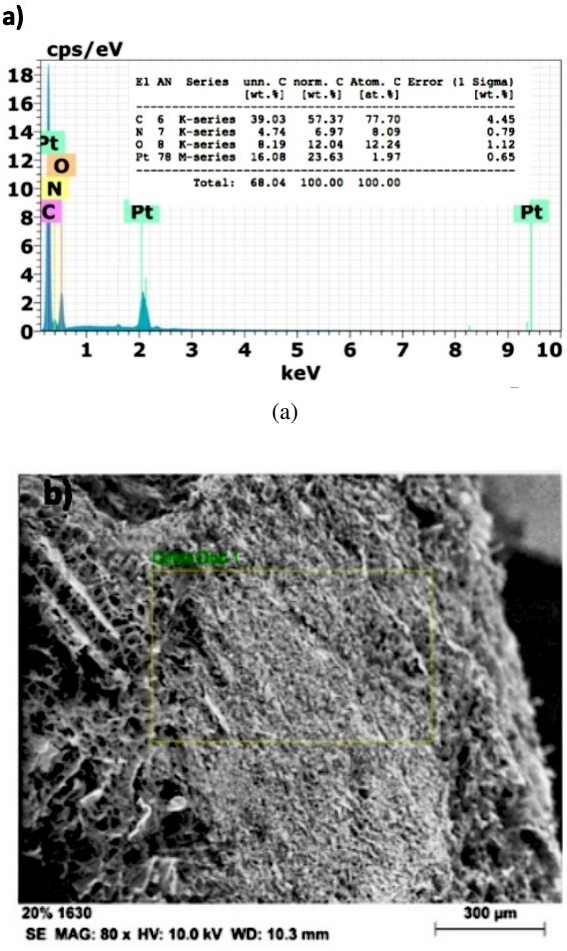


Fig. 4. FTIR-ATR spectra of all hydrogel samples

Table 3 shows the hydrogels' chemical composition using EDS analysis. All samples contained carbon, oxygen, and platinum, which was the element used for coating. This result suggests that the synthesis did not incorporate impurities such as sulfur from the redox initiator. Nitrogen was detected only in samples with a relatively low concentration of MBA (hydrogels groups H1.A, H1.0, H2.A, and H2.0), probably because the other samples had a large number of pores, so nitrogen detection was impaired. Figure 5 shows the EDS spectrum and the corresponding SEM image of the hydrogel H1.A.



(a)

(b)

Fig. 5. (a) EDS spectrum of hydrogel H1.A and (b) image of the region analyzed by EDS

III.3. X-Ray Diffraction

All samples showed an amorphous XRD halo, characteristic of PNIPAAm (Figure 6). Crystalline peaks were observed in hydrogels H2.0, H3.0, and H4.0 groups. This suggests that these hydrogels had crystalline regions not described in the literature, which could be an indication of a trend in the polymer chain to be organized. The degrees of crystallinity, determined by the Ruland method [19], were 7.3%, 5.5%, and 5.6% for hydrogels H2.0, H3.0, and H4.0, respectively.

III.4. Morphology

Figure 7 shows different hydrogel morphologies. Samples from H2.0, H3.0, and H4.0 groups display some degree of organization. These results can be associated with the small movements of their molecules during synthesis. The smaller the movement, the lower will be the entropy of the system. This behavior allows for organized polymerization [22]. The lamellar structure was observed in samples with many pores. The H4 hydrogel showed a structure with a greater formation of layers. The distance between the layers is approximately 10 µm.

The sample of H1.0 does not show organized regions (Figure 8), with many cavities in some regions. This is consistent with XRD results since its diffractogram does not have crystalline peaks.

All synthesized samples with magnetic stirring

Table 3. Semiquantitative chemical composition (wt%) of the samples using EDS analysis

Groups	Carbon	Oxygen	Nitrogen	Platinum
H1.A	77.70	8.09	12.24	1.97
H1.0	72.51	4.86	3.93	18.70
H2.A	74.76	4.00	0.05	21.20
H2.0	80.19	10.90	5.42	3.48
H3.A	75.76	6.02	0	18.21
H3.0	73.65	7.03	0	19.32
H4.0	65.41	7.81	0	26.78

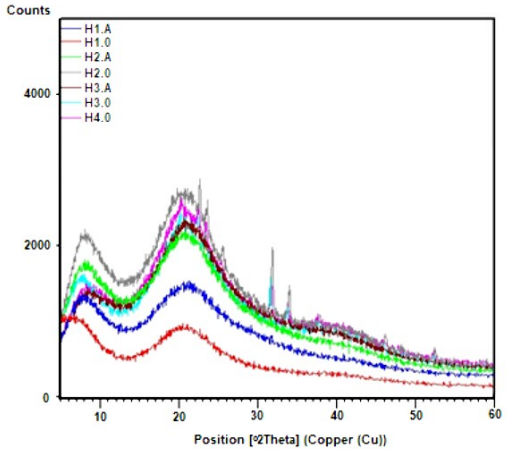


Fig. 6. XRD patterns of the hydrogels.

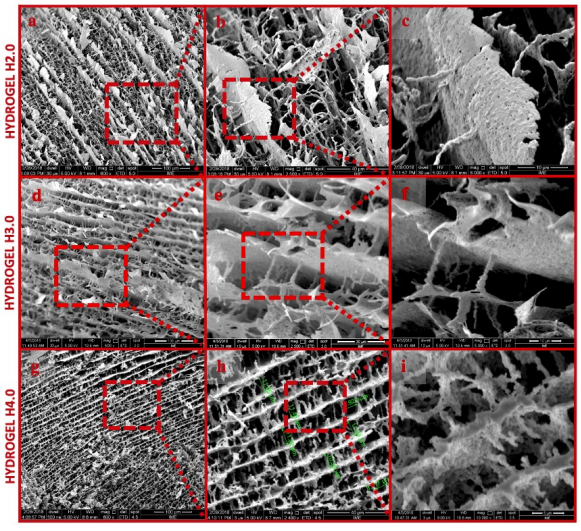


Fig. 7. SEM morphologies of the samples of H2.0, H3.0, and H4.0. Magnification of the sample of H2.0: (a) 600 ×; (b) 2,500 ×; (c) 8,000 ×. Magnification of the sample of H3.0: (d) 600 ×; (e) 2,500 ×; (f) 5,000 ×. Magnification of the sample of H4.0: (g) 600 ×; (h) 2,400 ×; (i) 10,000 ×

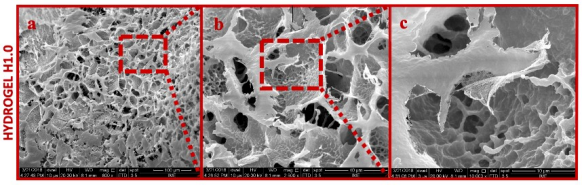


Fig. 8. Morphologies of the sample of H1.0. Magnifications: (a) 600 ×; (b) 2,500 ×; (c) 10,000 ×.

during the polymerization process (H1.A, H2.A, and H3.A) showed no ordering and different morphologies with cavities of different sizes (in Figure 9), so these results corroborate the oscillatory swelling capacity. The sample of H1.A had two different regions, one with large cavities and another similar to a spiderweb. Sample H2.A displayed diagonal layers and cavities of several sizes. Both H1.A and H2.A showed a nonporous surface. The sample of H3.A showed a globular surface with a convoluted morphology that gives it a spongy appearance. Of the three, H3.A is the one with the largest swelling capacity because the bigger the cavities the more solvent would be warehoused. Magnetic agitation has been an indication of the influence of entropy on the system: when the hydrogel is not at rest during the synthesis process, entropy increases, and so does the number of events that polymer chains have to connect to establish a diversified number of polymeric bridges and create hydrogels with different behaviors.

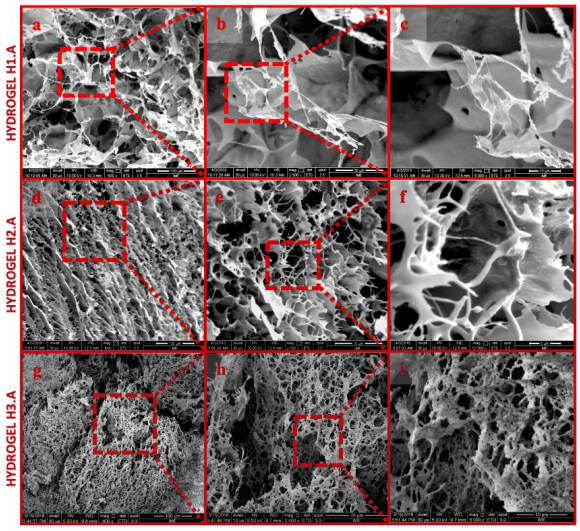


Fig. 9. Morphologies of the samples of H1.A, H2.A, and H3.A. Magnification of the sample of H1.A: (a) 600 ×; (b) 2,500 ×; (c) 5,000 ×. Magnification of the sample of H2.A: (d) 600 ×; (e) 2,500 ×; (f) 10,000 ×. Magnification of the sample of H3.A: (g) 600 ×; (h) 2,500 ×; (i) 8,000 ×

III.5. Thermogravimetric Analysis

Thermogravimetric analysis of the hydrogels (Figure 10) showed that the material had degraded in different events. All hydrogels had a mass decrease at a temperature below 150°C, which is due to the loss of the water absorbed by the sample. The samples of H2.A and H3A had only two degradation events, meaning that these hydrogels have chains with similar size distribution. The samples of H1.A, H1.0, H2.0, H3.0, and H4.0 had three degradation events. The degradation events are shown in Table 4, with values of T_{max} and T_{peak}. The second degradation event occurred below 300°C for the samples of H1.A, H1.0, H3.0, and H4.0; for the samples of H2.A and H3.A, they happened around 380°C. The third event occurred below 415°C for the samples of H1.A, H1.0, H2.0, H3.0, and H4.0. According to Lucas et al. [23], this degradation event can be an indication that these hydrogels have smaller chains with a wider size distribution. The temperature at which this degradation event occurs depends on the chain length: the higher the value of T_{peak}, the longer the chains and the more rigid the structure. The sample of H2.0 had the largest value of T_{peak}, 412°C and the smallest swelling capacity, showing that it has the longest and most rigid chains. The sample of H4.0 had the smallest value of T_{peak}, 376°C, suggesting that it had the shortest chains with a highly crosslinked network according to its small swelling capacity. Samples synthesized with stirring (H2.A and H3.A) showed greater thermal stability than those synthesized without stirring. With respect to swelling capacity, the sample of H2.A is more rigid than the sample of H3.A, and this is confirmed by thermogravimetric analysis, since for the second event, T_{peak} of the sample of H2.A is 8°C higher than for the samples of H3.A. Moreover, these hydrogels were the most stable with values of T_{peak} for the first event of 104°C and 111°C, respectively.

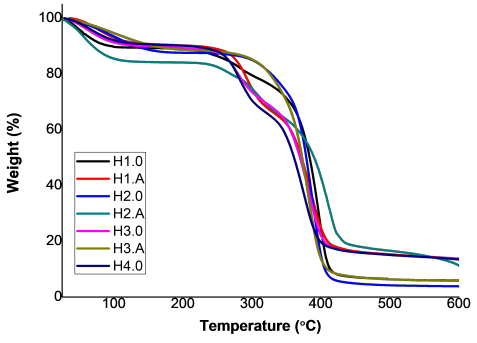


Fig. 10. PNIPAAm hydrogels' thermogravimetric analysis (TGA)

IV. Conclusion

The main purpose of this study was to analyze the influences of crosslinker agent concentration, initiators, and magnetic stirring on the polymerization process during the syntheses of PNIPAAm smart hydrogels and to determine which characteristics these compounds can present. It was concluded that the hydrogels synthesized with magnetic stirring had a larger swelling capacity than the hydrogels synthesized without stirring. This capacity is due to the fact that these samples (H2.A and H3.A) have polymeric chains with different

Table 4. Thermogravimetric data of the hydrogels

Sample	1st event		2nd event			3rd event		
	T_{peak} (°C)	Residue	T_{max} (°C)	T_{peak} (°C)	Residue	T_{max} (°C)	T_{peak} (°C)	Residue
H1.A	74	4%	265	291	20%	349	381	61%
H1.0	54	5%	262	286	18%	360	397	71%
H2.A	104	7%	342	389	67%	-	-	-
H2.0	56	6%	271	307	20%	378	412	69%
H3.A	111	6%	346	381	62%	-	-	-
H3.0	61	4%	259	279	21%	350	383	66%
H4.0	65	4%	260	281	23%	351	376	65%

sizes and crosslinking degrees. Furthermore, the crosslinking agent and initiator concentrations influenced the degree of swelling and stiffness of the hydrogels, as the higher, the crosslinking agent or initiator, the more rigid is the hydrogel. The H2.0 hydrogel with 84.4 mol % of NIPAM and 15.8 mol % of MBA had the highest degree of crosslinking, the least swelling capacity, and the highest thermic stability, although it does not have the highest crosslink agent concentration. Then, the higher initiator concentration developed a rule more important than a higher crosslink agent concentration, because the combination of the redox initiator and the crosslinker concentration was the best on the H2.0 sample. The XRD, NMR, FTIR, and EDS indicate that all seven hydrogels were obtained without the presence of impurities and they have different characteristics, but all of them presented a 3-D morphology with different quantities of cavities and porosity on the surface. As a final point, H2.0 and H4.0 (78.9 mol % of NIPAM and 15.7 mol % of MBA) were the most promising for biomedical applications, mainly as a scaffold for bone growth, due to their high thermal stability, adequate 3D surface morphology, and shrinking-swelling property.

Conflicts of Interest:

The authors declare that they have no known competing financial interests or personal relationships that could appear to influence the work reported in this paper.

Acknowledgements

The authors thank the Instituto de Macromoléculas (IMA/UFRJ-Brazil) for help with the TGA measurements, the Universidade Federal Fluminense (UFF-Brazil) for help with the XRD measurements, and the Brazilian Agencies CNPq, FAPERJ, and CAPES for financial support.

References

[1] Rico-Llanos GA, Borrego-González S, Moncayo-Donoso M, Becerra J, Visser R. Collagen type I biomaterials as scaffolds for bone tissue engineering. Polymers. 2021;13(4):599. doi:10.3390/polym13040599.

[2] Haq MA, Su Y, Wang D. Mechanical properties of PNIPAM based hydrogels: a review. Mater Sci Eng C. 2017;70(1):842–855. doi:10.1016/j.msec.2016.09.081.

[3] Chitra, V. Diagnosis, screening and treatment of osteoporosis–a review. Biomed Pharmacol J. 2021;14(2):567–575. doi:10.13005/bpj/2159.

[4] Cieza A, Causey K, Kamenov K, Hanson SW, Chatterji S, Vos T. Global estimates of the need for rehabilitation based on the Global Burden of Disease study 2019: a systematic analysis for the Global Burden of Disease Study 2019 [published correction appears in Lancet. 2020 Dec 4]. Lancet. 2021;396(10267):2006-2017. doi:10.1016/S0140-6736(20)32340-0.

[5] Amukarimi S, Ramakrishna S, Mozafari M. Smart biomaterials—a proposed definition and overview of the field. Curr Opin Biomed Eng. 2021;19(100311). doi.org/10.1016/j.cobme.2021.100311.

[6] Montoyal C, Du Y, Anthony L, Gianforcaro AL, Orrego S, Yang M, et al. On the road to smart biomaterials for bone research: definitions, concepts, advances, and outlook. Bone Research 2021;9(1):12. doi.org/10.1038/s41413-020-00131-z.

[7] Lorenzo RA, Carro AM, Concheiro A, Alvarez-Lorenzo C. Stimuli-responsive materials in analytical separation. Anal Bioanal Chem. 2015;407:4927–4948. doi:10.1007/s00216-015-8679-1.

[8] Łabowska MB, Cierluk K, Jankowska AM, Kulbacka J, Detyna J, Michalak I. A review on the adaption of alginate-gelatin hydrogels for 3D cultures and bioprinting. Materials. 2021;14(4):858. doi:10.3390/ma14040858.

[9] Alexander A, Ajazuddin, Khan J, Saraf S, Saraf S. Polyethylene glycol (PEG)-Poly(N-

isopropylacrylamide) (PNIPAAm) based thermosensitive injectable hydrogels for biomedical applications. Euro J Pharm Biopharm. 2014;88(3):575–585. doi: 10.1016/j.ejpb.2014.07.005.

[10] Sikdar P, Uddin M, Dip TM, Islam S, Hoque MS, Dhar AK, et al. Recent advances in the synthesis of smart hydrogels. Mater Adv. 2021;2:4532–4573. doi:10.1039/D1MA00193K.

[11] He W, Ma Y, Gao X, Song J. Application of Poly(N-isopropylacrylamide) as thermosensitive smart materials. J Phys: Conf Ser. 2020;1676(1):012063. doi:10.1088/1742-6596/1676/1/012063.

[12] Koetting MC, Peters JT, Steichen SD, Peppas NA. Stimulus-responsive hydrogels: theory, modern advances, and applications. Mater Sci Eng: R Rep. 2015;93:1–49. doi:10.1016/j.mser.2015.04.001.

[13] Icriverzi M, Rusen L, Sima LH, Moldovan A, Brajnicov S, Bonciu A, et al. In vitro behavior of human mesenchymal stem cells on poly(N-isopropylacrylamide) based biointerfaces obtained by matrix-assisted pulsed laser evaporation. Applied Surface Science. 2018;440:712–724. doi:10.1016/j.apsusc.2018.01.200.

[14] Queiroz PM. Síntese e caracterização de hidrogéis superabsorventes obtidos a partir da copolimerização de acrilamida, n-isopropilacrilamida e metacrilato de sódio. Belo Horizonte: Universidade Federal de Minas Gerais; 2010.

[15] Matzelle TR, Geuskens G, Kruse N. Elastic properties of poly(N-isopropylacrylamide) and poly(acrylamide) hydrogels studied by scanning force microscopy. Macromolecules. 2003;36(8):2926–2931. doi:10.1021/ma021719p.

[16] Aquada FA, Muniz EC, Vaz CMP, Mattoso LHCC. Correlation between parameters of swelling kinetic with network and hydrophilic characteristics of polyacrylamide and methylcellulose hydrogels. Química Nova, 2009;32(6):1482–1490. doi:10.1590/S0100-40422009000600023.

[17] Ribeiro CA., Martins MVS, Bressiani AH, Bressiani JC, Leyva ME, de Queiroz AAA. Electrochemical preparation and characterization of PNIPAM-HAp scaffolds for bone tissue engineering. Mater Sci Eng C. 2017;81:156–166. doi:10.1016/j.msec.2017.07.048.

[18] Hong TT, Okabe H, Hidaka Y, Hara K. Radiation synthesis and characterization of superabsorbing hydrogel from natural polymers and vinyl monomer. Environ Pollut. 2018;242(Pt B):1458–1466. doi:10.1016/j.envpol.2018.07.129.

[19] Ruland W. X-ray determination of crystallinity and diffuse disorder scattering. Acta Crystallographica. 1961;14:1180–1185. doi:10.1107/S0365110X61003429.

[20] Pavia DL, Lampman GM, Kriz G, Vyvyan JA. Introduction to spectroscopy. City: Cengage learning; 2014.

[21] Wang N, Ru G, Wang L, Feng J. 1H MAS NMR studies of the phase separation of poly (N-isopropylacrylamide) gel in binary solvents. Langmuir. 2009;25(10):5898–5902. doi:10.1021/la8038363.

[22] Zhang R, Lee B, Stafford CM, Douglas JF, Dobrynin AV, Bockstaller MR, Karim, A. (2017) Entropy-driven segregation of polymer-grafted nanoparticles under confinement. Proc Natl Acad Sci. 2017;114(10):2462–2467. doi:10.1073/pnas.1613828114.

[23] Lucas EF, Soares BG, Monteiro, EE. Caracterização de polímeros: determinação de peso molecular e análise térmica. Rio de Janeiro: E-papers Serviços Editoriais; 2001.

Received 2022-03-14
Accepted 2022-05-31